ANALYTICAL AND EXPERIMENTAL INVESTIGATION ON ADVANCED COMPOSITE WING BOX STRUCTURES IN BENDING INCLUDING EFFECTS OF INITIAL IMPERFECTIONS AND CRUSHING PRESSURE

E. ANTONA and G. ROMEO
Dept. of Aerospace Engineering, Polytechnic Institute of Turin, Italy

Abstract

When bending loads are applied on a wing box beam, the bending curvature, associated with longitudinal load, causes a distributed load perpendicular to both the upper and lower wing box panel resulting in a crushing pressure. Deformations of the wing box compression panel are analytically investigated using a differential equation of the orthotropic plate; lateral pressure and initial imperfections are simulated in the analysis by a Fourier series. Particularly on stiffened panels, these can both play an important role on strain distribution affecting the longitudinal load at which buckling could occur.

Experimental results on advanced composite wing box beams in bending showed remarkable deformations of the panels (particularly the compressed panel) in a direction normal to their barycentric surface affecting both local stress values and the failure load value of the structures.

As an effect of the crushing pressure, a blade stiffened panel wing box failed at a load greater than the predicted buckling load.

As an effect of the initial imperfection, an unstiffened panel wing box buckled at a bending moment greater than the predicted buckling load.

I. Introduction

Since the beginning of the 1970's, increasing attention has been paid to advanced composite materials for aerospace structures because of the mass reduction they can permit; application of advanced composites in the primary structures, including the wing structure, is planned for most commercial transport aircraft designed today.

Some experimental and analytical results are available in literature on composite stiffened panels under combined loads, with different constraints at the edges and including bow-type initial imperfection. However, the panels themselves are considered separately from the main structure; indeed, boundary conditions at the edges are not always well known and deformations could be induced at the edges by the other sub-structures. Furthermore, additional loads are created on a wing box compression panel when bending loads are applied on the beam; bending curvature, associated with longitudinal load, causes a distributed load perpendicular to both the upper and lower wing box panels resulting in a crushing pressure. The bending curvature will not be constant in the transverse direction , but will reach a maximum value at the center of the two webs. This perpendicular load can play an important role in the strain distribution of each element (skin and stiffeners) affecting the longitudinal load at which buckling could occur [1] .

Deformations of wing box compression panels are analytically investigated using a differential equation of the orthotropic plate [2] . Crushing pressure and initial shape imperfections present, from a mathematical point of view, a contribution to the known terms of the equation and are simulated in the analysis by a Fourier series.

The wing box beams taken into consideration are mainly made up of two panels and two webs, although transverse ribs can also be taken into account . Using the Engineer's Theory of Bending (ETB), deflections of the beam are easily evaluated along the webs; however, deflections of the panels, particularly the compressed panel, are considerably different from those evaluated by the ETB even before buckling occurs. Both analytical and experimental results showed such different deformations.

II. Theoretical Analysis

The deflection of the barycentric surface of the wing box panels (Fig.1) is evaluated using the present analysis and compared with the ETB. Beams are assumed to have, between two ribs, a uniform cross-section, constant material mechanical properties and to be subjected to a uniform load; it is also assumed that at the sides the deflections are evaluated by the ETB.

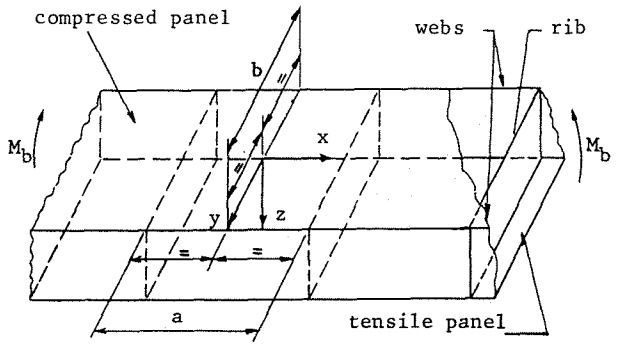

FIGURE 1

Each panel is analytically investigated using a differential equation of an orthotropic plate; indeed, anisotropic bending stiffnesses D_{16} and D_{26} are not null when angle-ply laminae are included in the laminates. In reference [3], it has been shown that a change of a few percent (up to 4%) could be introduced in the buckling load neglecting anisotropic stiffnesses on the buckling of symmetrically laminated composite plates loaded in compression.

Simply supported edge conditions are considered between the panels and webs. Although in practical application simply supported edge conditions are considered between the panels and ribs, it is supposed that ribs could react to panel rotation by a moment proportional to the reaction constant of the rib.

Within the hypothesis of small deflections, the general differential equation for the deflection of an orthotropic plate having initial imperfections and submitted to longitudinal load and lateral pressure, was:

$$D_1\frac{\partial^4 w}{\partial x^4} + 2D_3\frac{\partial^4 w}{\partial x^2\partial y^2} + D_2\frac{\partial^4 w}{\partial y^4} - N_x\frac{\partial^2 w}{\partial x^2} = p + N_x\frac{\partial^2 w_o}{\partial x^2} \quad (1)$$

The orthotropic stiffnesses involved are the longitudinal and transverse bending stiffnesses D_1 and D_2, respectively, and the twisting stiffness D_3. The lateral pressure involved is correlated to the bending moment applied.

Surface deflection, lateral pressure and initial imperfection was represented [2,4] by:

$$w = \sum_{n=o}^{\infty} \phi_n \cos(1+2n)\frac{\pi y}{b} + \sum_{n=1}^{\infty} \psi_n \operatorname{sen} 2n\frac{\pi y}{b} \quad (2)$$

$$p = \frac{4p}{\pi}\sum_{n=o}^{\infty}\frac{(-1)^n}{1+2n}\cos(1+2n)\frac{\pi y}{b} \quad (3)$$

$$w_o = \sum_{n=o,1..} \phi_{on}\cos(1+2n)\frac{\pi y}{b} + \sum_{n=1,2..} \psi_{on}\operatorname{sen} 2n\frac{\pi y}{b} \quad (4)$$

in which ϕ_n, ψ_n, ϕ_{on} and ψ_{on} are functions of x to be determined; ϕ_{on} and ψ_{on} are assumed to be g-degree polynomials in x. By substitution, the following set of ordinary differential equations was obtained:

$$\frac{d^4\phi_n}{dx^4} - 4A_n\frac{d^2\phi_n}{dx^2} + 4B_n\phi_n = 4F + \frac{N_x}{D_1}\frac{d^2\phi_{on}}{dx^2} \quad (5)$$

when n=0,1,2,....

$$\frac{d^4\psi_n}{dx^4} - 4A_n\frac{d^2\psi_n}{dx^2} + 4B_n\psi_n = \frac{N_x}{D_1}\frac{d^2\psi_{on}}{dx^2} \quad n=1,2,3,... \quad (6)$$

where:

$$A_n = \frac{1}{2}\left(\frac{\pi}{b}\right)^2\frac{D_3}{D_1}m^2 + \frac{N_x}{4D_1}\ ;\ B_n = \frac{1}{4}\left(\frac{\pi}{b}\right)^4\frac{D_2}{D_1}m^4$$

$$F_n = \frac{(-1)^n}{1+2n}\frac{p}{\pi D_1}$$

and m = (1+2n) when applied to eq.(5)
m = 2n when applied to eq.(6)

Equation 5, which gives the symmetrical harmonics, was solved in reference [6] by assuming $\phi_n = e^{\lambda x}$; the following results were obtained for three different load ranges:

1) When

$$-2\left(\frac{\pi}{b}\right)^2 m^2(D_3 + \sqrt{D_1D_2}) < N_x < 2\left(\frac{\pi}{b}\right)^2 m^2(\sqrt{D_1D_2} - D_3)$$

$$\phi_n = C_1\cos P_n x\cosh Q_n x + C_2\sin P_n x\sinh Q_n x + C_3\cos P_n x\sinh Q_n x + C_4\sin P_n x\cosh Q_n x + F_n/B_n + \Phi_o + \Phi_1 x + ... + \Phi_{(g-2)}x^{(g-2)}$$

where:

$$P_n = \sqrt{-A_n + \sqrt{B_n}}\ ;\ Q_n = \sqrt{A_n + \sqrt{B_n}}$$

2) When

$$N_x \leq -2\left(\frac{\pi}{b}\right)^2 m^2(D_3 + \sqrt{D_1D_2})$$

$$\phi_n = C_1\cos R_n x + C_2\cos S_n x + C_3\sin R_n x + C_4\sin S_n x + F_n/B_n + \Phi_o + \Phi_1 x + ...+ \Phi_{(g-2)}x^{(g-2)}$$

where:

$$R_n = \sqrt{-A_n + \sqrt{B_n}} + \sqrt{-A_n - \sqrt{B_n}}\ ;$$

$$S_n = \sqrt{-A_n + \sqrt{B_n}} - \sqrt{-A_n - \sqrt{B_n}}$$

3) When

$$N_x \geq 2\left(\frac{\pi}{b}\right)^2 m^2(\sqrt{D_1D_2} - D_3)$$

$$\phi_n = C_1\cosh U_n x + C_2\cosh V_n x + C_3\sinh U_n x + C_4\sinh V_n x + F_n/B_n + \Phi_o + \Phi_1 x + ...+ \Phi_{(g-2)}x^{(g-2)}.$$

where

$$U_n = \sqrt{A_n + \sqrt{B_n}} + \sqrt{A_n - \sqrt{B_n}}$$

$$V_n = \sqrt{A_n + \sqrt{B_n}} - \sqrt{A_n - \sqrt{B_n}}$$

Similar expressions in ψ_n, which gives the antisymmetrical harmonics, were obtained by solving equation 6, except for the terms containing the pressure load.

The integration constants C_i are determined by the boundary conditions associated with the panel. Wing box deflections are then determined as the applied load increases towards the critical value.

III. Experimental Tests

Starting from the above consideration, pure bending tests were carried out on wing box beams; graphite/epoxy prepreg material was used for manufacturing the specimens and these were cured by an autoclave controlled pressure cycle.

One specimen had blade stiffened cross-section panels with a lamina stacking sequence and dimensions as shown in Fig.2a; wing box length,

excluding the fittings, was 69 cm. A second specimen had unstiffened orthotropic panels (Fig.3a) and was 70 cm long.

Suitable fittings were bolted at the ends of the wing boxes in order to attach them to the bending machine (Fig.2). Specimens were bolted by two clamps hinged to the frame by four rods; a hydraulic jack was hinged to the other side of each clamp so that the bending moment was applied step by step. Deflection data at different load levels were taken by means of a dial deflectometer which ran on a slideway for a length of 42.5 cm and was connected to an x-y recorder. Longitudinal strains were measured at the half length by several strain gages placed back-to-back both for the skin and the stiffeners. In such a way, any local phenomenon can be recognized by the strain reversal method.

Blade-stiffened panels wing box.

A slight difference was measured between the thicknesses of the skin and stiffeners of the compression and tension panels (Fig.2a). The wing box mass was 5 kg.

The deflection curves were measured along the sides and in the longitudinal middle section of the wing box compression panel; they are drawn in Fig.2b for different values of the bending moment. A remarkable difference can be seen very clearly from this picture, as well as from the axonometric view, as an effect of the lateral pressure.

The wing box deflection curves analytically determined by the present theory are drawn in Fig.2c for different values of the bending moment both in the longitudinal lateral and middle sections; these values are compared with the experimental curves drawn at the same bending moment. The theoretical and experimental results are in very close agreement up to a bending moment of 17.95 kNm; after that , an ever-increasing difference was obtained. This agrees with the theoretical hypothesis of an infinite deflection as the applied load reaches the critical value. According to the present theory an overall buckling should have occurred at a bending moment of 23.62 kNm; if submitted only to longitudinal load, buckling should have occurred at a longitudinal load of 435 N/mm, corresponding to a bending moment of 26.11 kNm. The local buckling loads of the skin and stiffeners as well as the torsional buckling load were much greater than the overall buckling load.

The surface strain data measured by the back-to-back strain gages placed both on the skin and stiffeners are plotted in Fig. 2d as a function of the applied bending moment. It is very clear from these pictures that, starting at a bending moment of 23.33 kNm, a strain reversal occurred in three of the stiffeners placed near the longitudinal middle section (strain gages 3-4, 5-6, 7-8); since both back-to-back strain gages of each of the three stiffeners behaved in the same way,

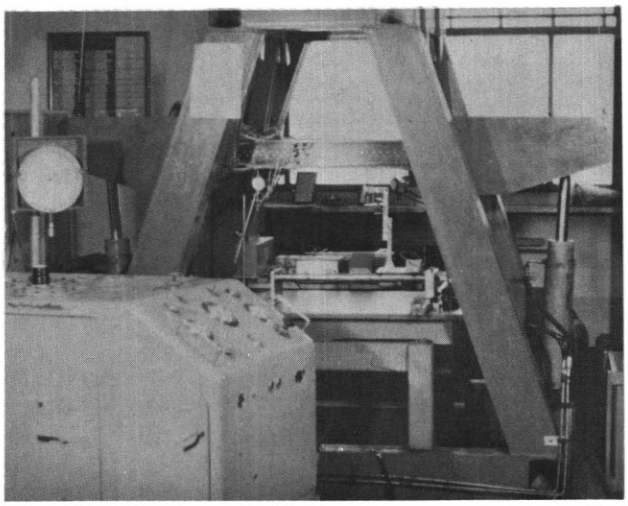

Test machine

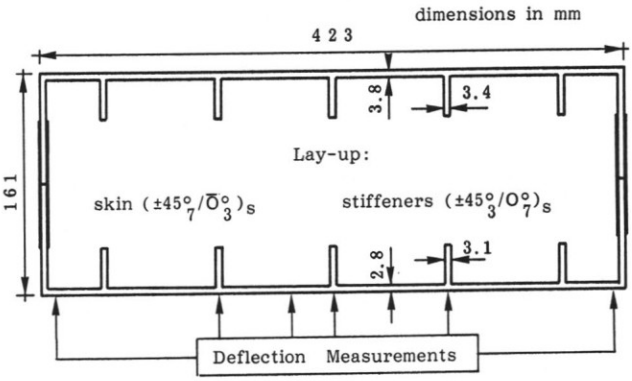

a) Stacking sequence and dimensions.

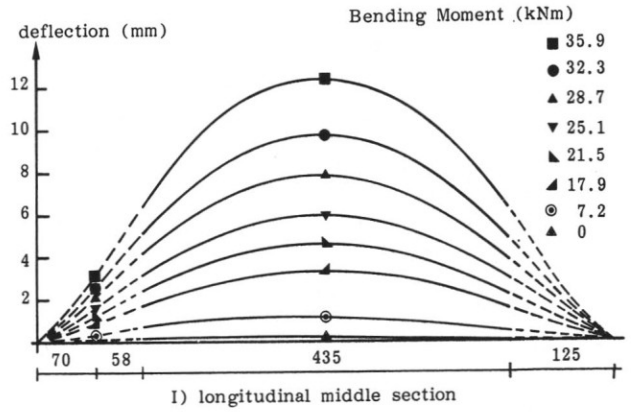

I) longitudinal middle section

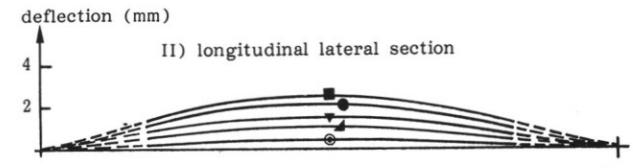

b) Experimental deflection curves of the compression panel for different values of the bending moment.

FIGURE 2. Blade-stiffened panels wing box under pure bending.

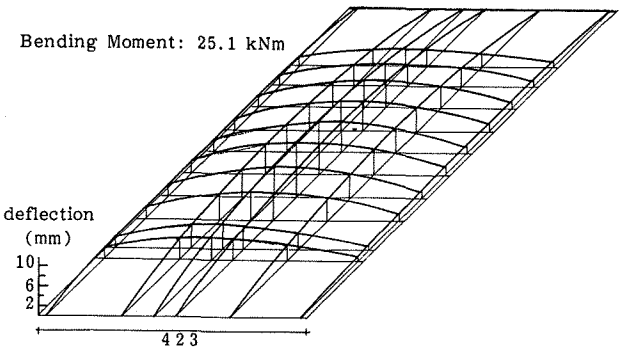

b)axonometric view at a bending moment of 25.1kNm

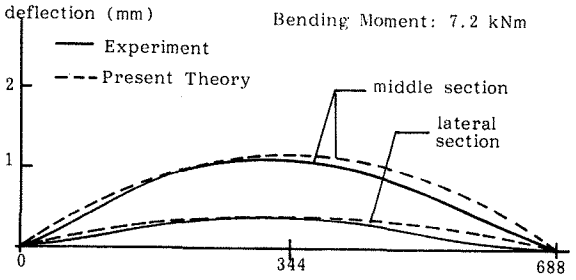

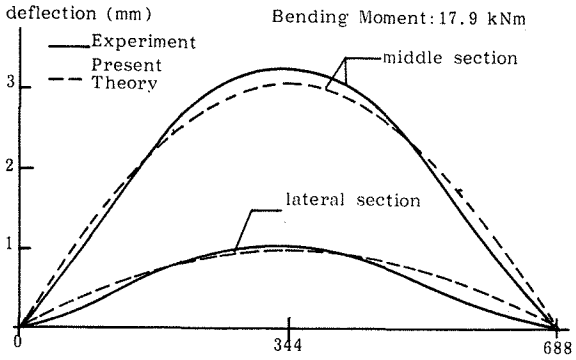

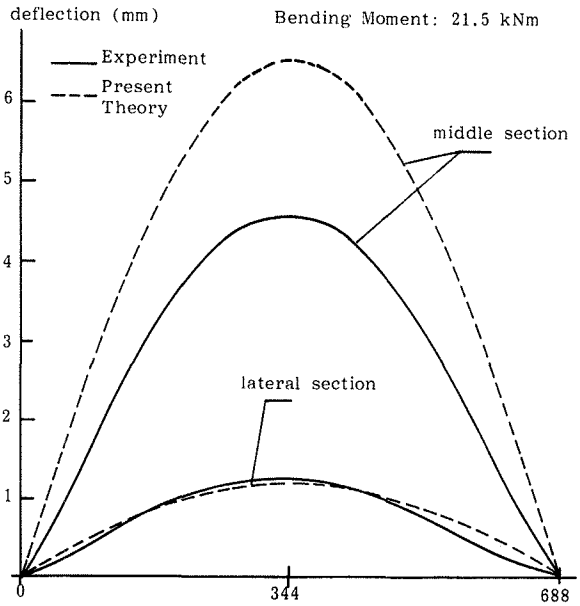

c)comparison between the theoretical and experimental results of the wing box deflection curves

FIGURE 2. continue.

local stiffener buckling is excluded. Indeed, as an effect of both bending curvature and lateral pressure, the stiffeners themselves were subjected to a local bending moment that drastically changed the hypothesis of a uniform compression longitudinal load on the panel. The stiffeners placed near the webs (strain gages 1-2) followed an almost linear behaviour up to the failure bending moment. An almost linear behaviour was also recorded for the skin up to the critical bending moment; after that, ever-increasing strains arose in the outer lamina of the laminate as an effect of the lateral pressure. A strain reversal seems to begin in the middle width of the skin (strain gages 15-16) at a bending moment of 39.5 kNm, the maximum value at which data were recorded.

An almost linear behaviour was recorded in the wing box tensile panel, both for the stiffeners (strain gages 27-28) and for the skin (strain gages 35-36); lateral pressure and bending curvature seem to affect the behaviour of the tensile panel only in strain values. In fact, since the compressed and tensile panels move closer, a reduction of the wing box bending stiffness leads to a higher strain distribution on the panel.

The wing box failed at a bending moment of 43.1 kNm (corresponding to a longitudinal load of 717 N/mm) by delamination of the compression skin at about 90mm from one end. Although the applied strains are not well known, since there were no strain gages placed in that area, it seems possible that failure happened as a result of the local buckling of the stiffeners.

An interesting comparison is possible with a very similar blade-stiffened panel tested under uniaxial compression [5]. The panel was six-stiffeners wide, 66.5cm long and slightly thicker than the wing box compression panel; the ends were simply supported and the sides were free. The specimen failed at a predicted Euler buckling load of 434 N/mm, which was very close to the local buckling load of the stiffners.

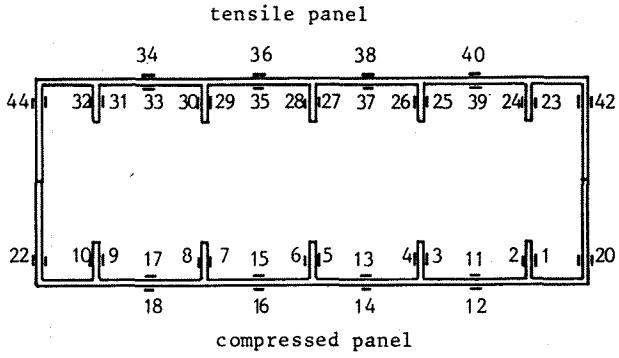

d) strain gages disposal

FIGURE 2. continue

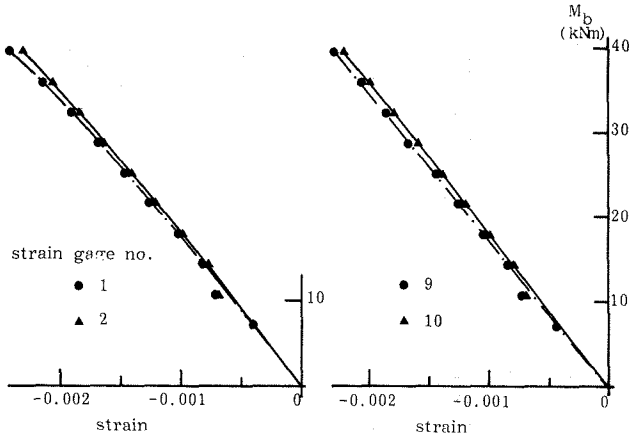

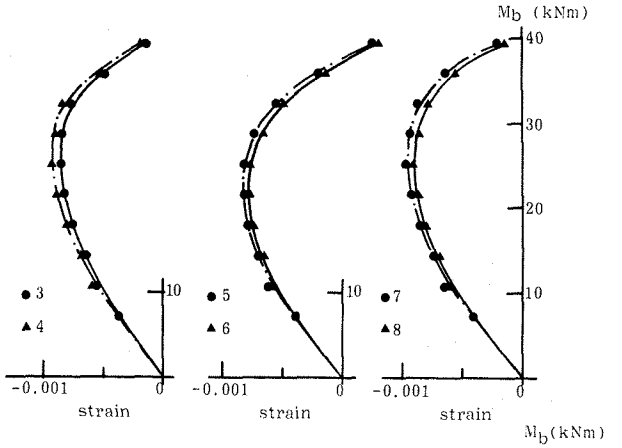

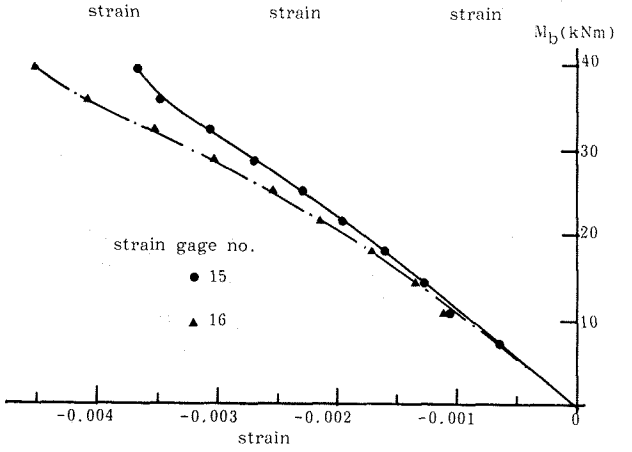

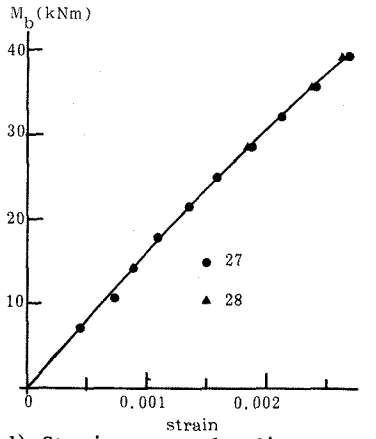

d) Strain versus bending moment curves for several back-to-back strain gages.

FIGURE 2. continue

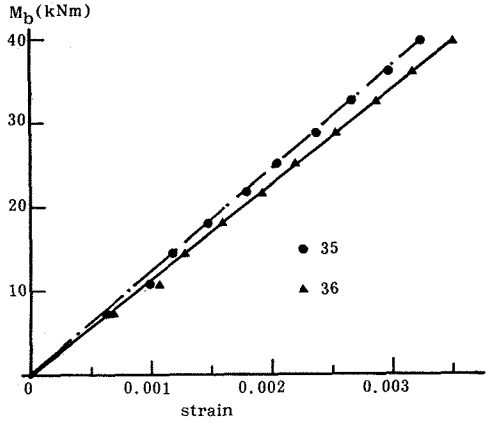

d) Strain versus bending moment curves.

FIGURE 2. Blade-stiffened panels wing box under pure bending. Conclude.

Unstiffened panels wing box.

The wing box mass was 6.5 kg. Experimental results are reported in Fig.3. The surface strain data measured by the back-to-back strain gages and computed membrane strain are plotted for several bending moment values (Fig.3b). Strain gages were placed on both panels and in the webs in the middle length only. A bow type initial imperfection was recorded in the compression panel and the highest value measured was 1 mm at the middle width and 0.1 mm at the edges (Fig.3d).

A maximum membrane strain of 0.00062 was achieved in the middle longitudinal section at a bending moment of 21.54 kNm, after this it began to reduce. High strains were recorded at the edges as the applied load increased. Based on the orthotropic buckling equations for a simply supported plate, buckling should have occurred in two half waves at a longitudinal strain of 0.00049; however, because the plate aspect ratio is 1.61, the nearest buckling form was one half wave at a longitudinal strain of 0.00063. From the bending moment versus strain curves (Fig.3c), a reversal is very clear in strain gage number 23 at a bending moment of 14.36 kNm which correspond to a membrane strain of 0.00046. This value was in very close agreement with the analytically predicted buckling strain of the plate; however, increasing the bending moment up to a value of 21.54 kNm produced the maximum membrane strain of 0.00062 and the panel had a half wavelength higher than the one corresponding to a two half wave symmetrical buckle mode. The difference between the load at which the strain reversal occurred and the load at which the maximum membrane strain occurred can be attributed to the distributed perpendicular load. In fact, it is very clear how, in the middle section of the tensile panel, the inner surface strain (gage 9) had a higher value than the outer one (gage 10); while at the edges the perpendicular load did not

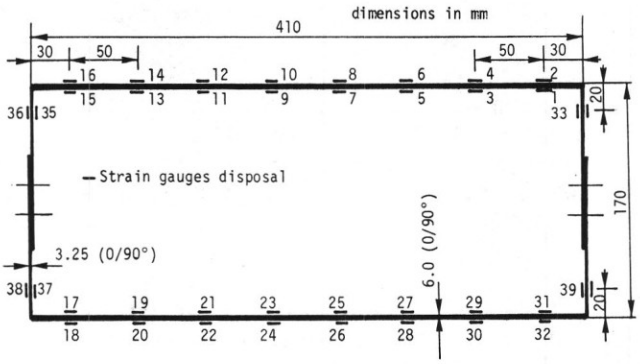

a) Stacking sequence, dimensions and strain gages disposal.

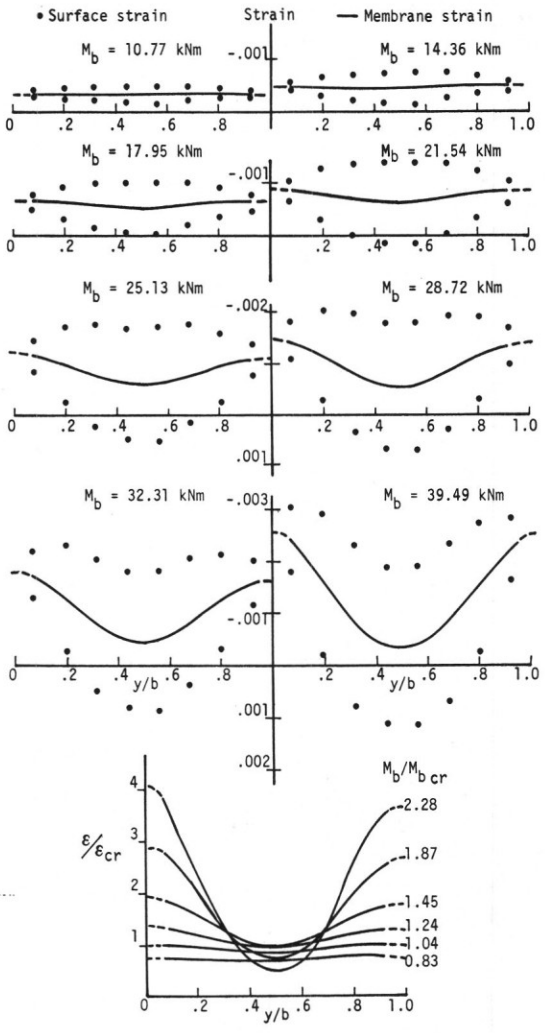

b) Surface and membrane strain curves for different values of the bending moment

FIGURE 3. Unstiffened panels wing box under pure bending.

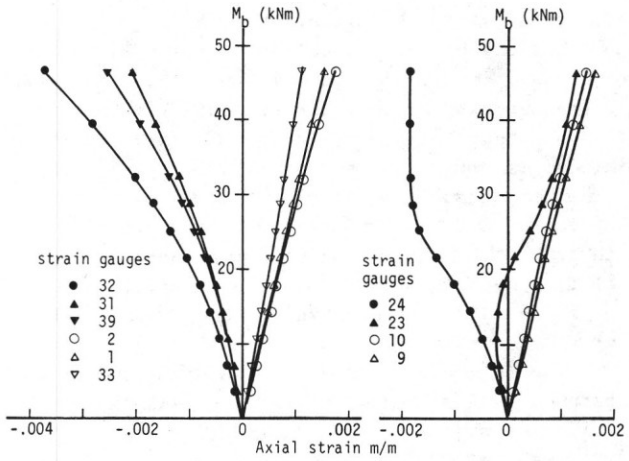

c) Strain versus bending moment curves for several back-to-back strain gages

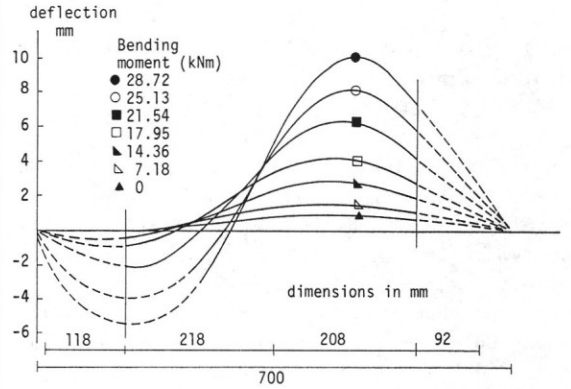

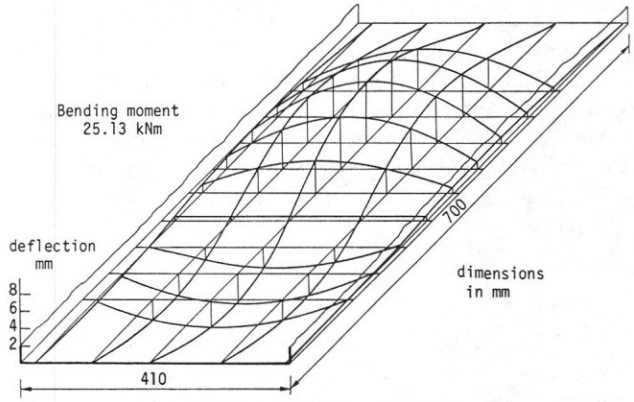

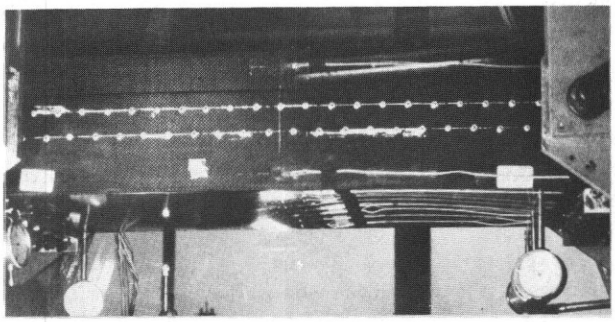

d) Experimental deflection curves of the compression panel for different values of the bending moment.

FIGURE 3. Unstiffened panels wing box under pure bending. Conclude.

affect the strain distribution.

The experimental buckling load was higher than the analytically determined one since the edge stiffening was, probably, different from the simple support hypothesis; however, it seems that the initial imperfection made buckling corresponding to a higher strain energy possible (barrel effect). Deflection curves taken near the webs showed a linear relation to the load, and in close relationship with the ETB, up to a bending moment of 21.54 kNm, beyond which the usual bending curvature was no longer kept.

The structure tested showed a remarkable postbuckling strength. No failure occurred at the maximum test load of 46.67 kNm and residual deformations were negligible.

Conclusion

The general differential equation for the deflection of an orthotropic plate was solved by representing the deflection, lateral pressure and initial imperfections using the Fourier series.

The deflections of the wing box compression panels are particularly affected by the crushing pressure caused by the beam bending curvature, resulting in much greater deflections than those analytically determined by the Engineer's Theory of Bending.

Consequently, the stress distribution in the individual elements of the structure is modified and the longitudinal load at which buckling occurred was proved to be different than the analytically determined load.

By the present theory this effect has been well evaluated; indeed, as the applied load increases to the critical value the deflections trend to an infinite value; since the present theory was developed within the hypothesis of small deflections it is no longer valid when deflections increase drastically.

Acknowledgements

The Authors acknowledge the efficacius cooperation of Dr.M. Bettinardi who gave its contribution in experimental work, practical measurements and data elaboration.

References

(1) ANTONA, E. and GABRIELLI, G.: An Experimental Investigation on Wing Box Beams in Bending. ICAS Paper No.70-83, Sept.1970.

(2) ANTONA, E. and PELAGALLI, P., Analisi Strutturale dei Cassoni Alari Bilongheroni Soggetti a Flessione in Campo Elastico (Structural Analysis of Two Spars Wing Boxes under Bending in the Elastic Field). Politecnico di Torino, Istituto di Progetto di Aeromobili, Report n.49, Dec.1968.

(3) NEMETE, M.P., Importance of Anisotropic Bending Stiffenesses on Buckling of Symmetrically Laminated Composite Plates Loaded in Compression. AIAA/ASME/ASCE/AHS 26th S.D.M. Conf., Orlando (USA) April 1985, Vol.I, pag.267.

(4) TIMOSHENKO, S.P. and GERE, J.M., Theory of Elastic Stability. McGraw-Hill, 1961.

(5) ROMEO, G., Experimental Investigation on Advanced Composite Stiffened Structures under Uniaxial Compression and Bending. AIAA/ASME/ASCE/AHS 26th S.D.M. Conference, Orlando (USA) April 1985, Vol.1, pag.283. To be published on AIAA Journal, August 1986.

(6) ANTONA, E., Effetto della Pressione Ortogonale e Fenomeni d'Instabilità Globale nei Pannelli Compressi dei Cassoni Alari Centinati Soggetti a Flessione (Effect of Orthogonal Pressure and Overall Buckling Phenomena on Wing Boxes Compression Panels under Bending). Politecnico di Torino, Istituto di Progetto di Aeromobili, Report n.40, Ott.1967.